Nanotechnology

ACCEPTED MANUSCRIPT • OPEN ACCESS

Ge(Sn) nano-island photodetectors with plasmonic antennas

To cite this article before publication: Viktoria Schlykow *et al* 2020 *Nanotechnology* in press https://doi.org/10.1088/1361-6528/ab91ef

Manuscript version: Accepted Manuscript

Accepted Manuscript is “the version of the article accepted for publication including all changes made as a result of the peer review process, and which may also include the addition to the article by IOP Publishing of a header, an article ID, a cover sheet and/or an ‘Accepted Manuscript’ watermark, but excluding any other editing, typesetting or other changes made by IOP Publishing and/or its licensors”

This Accepted Manuscript is **© 2020 The Author(s). Published by IOP Publishing Ltd.**.

As the Version of Record of this article is going to be / has been published on a gold open access basis under a CC BY 3.0 licence, this Accepted Manuscript is available for reuse under a CC BY 3.0 licence immediately.

Everyone is permitted to use all or part of the original content in this article, provided that they adhere to all the terms of the licence https://creativecommons.org/licences/by/3.0

Although reasonable endeavours have been taken to obtain all necessary permissions from third parties to include their copyrighted content within this article, their full citation and copyright line may not be present in this Accepted Manuscript version. Before using any content from this article, please refer to the Version of Record on IOPscience once published for full citation and copyright details, as permissions may be required. All third party content is fully copyright protected and is not published on a gold open access basis under a CC BY licence, unless that is specifically stated in the figure caption in the Version of Record.

View the article online for updates and enhancements.

This content was downloaded from IP address 77.220.194.92 on 18/05/2020 at 12:54

1 2 3 4 5 6 7 8 9 10 11 12 13 14 15 16 17 18 19 20 21 22 23 24 25 26 27 28 29 30 31 32 33 34 35 36 37 38 39 40 41 42 43 44 45 46 47 48 49 50 51 52 53 54 55 56 57 58 59 60

Ge(Sn) nano-island/Si heterostructure photodetectors with plasmonic antennas

Viktoria Schlykow [1,2], Costanza Lucia Manganelli [2], Friedhard Römer [3], Caterina Clausen [4], Lion Augel [5,4], Jörg Schulze [4], Jens Katzer [2], Michael Andreas Schubert [2], Bernd Witzigmann [3], Thomas Schroeder [6], Giovanni Capellini [2,7] and Inga Anita Fischer [8]

[1] Peter Grünberg Institute (PGI 10), Forschungszentrum Jülich, Wilhelm-Johnen-Straße, 52425, Jülich, Germany
[2] IHP – Leibniz-Institut für innovative Mikroelektronik, Im Technologiepark 25, D-15236 Frankfurt (Oder), Germany
[3] Computational Electronics and Photonics Group, University of Kassel, Wilhelmshöher Allee 71, 34121 Kassel, Germany
[4] Institut für Halbleitertechnik (IHT), Universität Stuttgart, Pfaffenwaldring 47, Stuttgart 70569, Germany
[5] Institute of micro and nano systems, BTU Cottbus, Platz der Deutschen Einheit 1, 03013 Cottbus, Germany
[6] Leibniz Institut für Kristallzüchtung, Max-Born-Straße 2, 12489 Berlin, Germany
[7] Dipartimento di Scienze, Università Roma Tre, Viale G. Marconi 446, I-00146 Rome, Italy
[8] Experimental Physics and Functional Materials, BTU Cottbus, Erich-Weinert-Str. 1, 03046 Cottbus, Germany

E-mail: v.Schlykow@fz-juelich.de

Abstract

We report on photodetection in deep subwavelength Ge(Sn) nano-islands on Si nano-pillar substrates, in which self-aligned nano-antennas in the Al contact metal are used to enhance light absorption by means of local surface plasmon resonances. The impact of parameters such as substrate doping and device geometry on the measured responsivities are investigated and our experimental results are supported by simulations of the three-dimensional distribution of the electromagnetic fields. Comparatively high optical responsivities of about 0.1 A/W are observed as a consequence of the excitation of localized surface plasmons, making our nano-island photodetectors interesting for applications in which size reduction is essential.

Keywords: nanoheteroepitaxy, photodetector, Ge, GeSn, localized surface plasmon resonances

Accepted Manuscript

1 2 3 4 5 6 7 8 9 10 11 12 13 14 15 16 17 18 19 20 21 22 23 24 25 26 27 28 29 30 31 32 33 34 35 36 37 38 39 40 41 42 43 44 45 46 47 48 49 50 51 52 53 54 55 56 57 58 59 60

Accepted Manuscript

1. Introduction

High performance photodetectors as a crucial building block for Silicon (Si) photonics are still a prominent field of research due to the importance of Si technology. One of the main limitations of photodetectors based on Si is their low responsivity. Alternative materials have, therefore, been at the focus of research efforts. While III-V compound semiconductors can be used as alternative materials for photodetectors, their integration on Si is costly and carries the risk of introducing contaminants into the fabrication process.

Germanium (Ge) is an indirect group IV semiconductor material, which is complementary metal-oxide-semiconductor (CMOS) compatible and its direct transition energy of 0.8 eV (corresponding to a wavelength of 1.55 µm) is only 140 meV above the indirect transition energy. This does not only make Ge much more suitable for application in optoelectronic devices compared to Si, it also allows for much higher absorption wavelengths compared to Si. Due to its enhanced intrinsic properties such as shorter absorption length, higher electron mobilities, faster response and lower power losses, Ge-based photodetectors are promising candidates for Si photonics applications [1]. Since high crystal quality is crucial for high-performance optoelectronic devices, the growth of high-quality Ge crystals was at the focus of early research efforts. Here, the development in the technological platforms in terms of growing Ge on Si substrates using e.g. graded buffers revolutionized the field of group IV based optoelectronics by reducing costs, achieving high device performance and moreover being CMOS compatible [2]. In a nanoheteroepitaxy (NHE) approach, material deposition is carried out on nano-patterned substrates to achieve high quality island growth without a graded buffer. In this approach the critical thickness, i.e. the thickness before introducing defects, is increased due to the partial shift of the accumulated strain energy in the islands to the substrate seeds, called substrate compliance effect, as well as the three-dimensional elastic relaxation mechanism [3], [4].

In addition to the utilization of innovative materials, the demand for a size reduction of photonic components is important in order to overcome the size mismatch between the electronic (nm-regime) and photonic parts (µm-regime). As a result of scaling down the active region to the nm-scale, photonic devices such as photodetectors can also be improved in speed through reduced capacitance, furthermore, their signal to noise ratio can be improved through lower dark currents [5]. However, quantum efficiency and responsivity can be expected to decrease at the same time, due to the decreased absorption in the reduced amount of active material. To compensate for the reduction in absorption while retaining the speed advantage of subwavelength-sized devices, plasmonic enhancement by so-called localized surface plasmon resonances (LSPRs), i.e. resonant excitations of the free electron gas of metallic nanoparticles by external electromagnetic fields, can be employed. The resonance wavelengths of the oscillations can be tuned to lie in the visible and near-infrared (NIR) spectrum [6], [7], [8], making them suitable for applications in biosensing [9], photovoltaics [10], [11] emitters [12] and photodetectors [13].

Up to now, plasmonically enhanced photodetectors have e.g. been demonstrated in the mid-infrared ($\lambda \approx 9$ µm) using metallic hole arrays [14], in the near-infrared (≈ 800 nm) using bullseye antennas [15], grating lenses [16], disc-shaped nanoantennas [17], [18] or dipole antennas [19] and in the visible using C-shaped nano-antennas [20]. The challenges of the aforementioned set-ups are that either the size of

1 2 3 4 5 6 7 8 9 10 11 12 13 14 15 16 17 18 19 20 21 22 23 24 25 26 27 28 29 30 31 32 33 34 35 36 37 38 39 40 41 42 43 44 45 46 47 48 49 50 51 52 53 54 55 56 57 58 59 60

the antennas themselves are in the µm-regime losing the advantages of size reduction or requiring cost intensive processing steps (e.g. nano-lithography).

Here, we report on the fabrication and electrooptical characterization of plasmon-enhanced Ge(Sn) nano-photodetectors, in which self-aligned Aluminum (Al) nano-antennas are combined with Ge(Sn) nano-islands. To form highly crystalline nano-islands, Ge(Sn) was deposited using molecular beam epitaxy (MBE) on nano-patterned Si wafers exploiting the advantages of NHE [3], [4]. In our devices, Al is simultaneously used as nano-antenna material and as the metal top contact of the device. We demonstrate comparatively high responsivities of about 0.1 A/W for incident light with a wavelength of ≈ 700 nm. Comparing experimental results concerning the effects of substrate doping and island size on the photoresponsivity of the Ge(Sn) nano-island photodetectors to finite element method (FEM) simulation results, we find that the wavelength-dependence of the responsivity can be correlated to LSPRs generated within our devices. This opens up promising avenues towards further increasing device responsivity and modifying its wavelength-dependence towards obtaining efficient nanoscale Ge-photodetectors directly integrated on Si.

2. Methods

2.1 Material and Device fabrication

Both Ge and GeSn nano-islands were grown using molecular beam epitaxy (MBE) on nano-patterned Si(001) substrates fabricated in a top to down fabrication process: Using photolithography and dry etching, square lattices of Si pillars were formed on Si(001) wafers with top diameters of 100 nm, a height of 100 nm and a lattice pitch of 230 nm. The Si nano-pillars were completely covered with SiO_2 deposited by plasma enhanced chemical vapor deposition. A chemical-mechanical-polishing (CMP) process was used as the final step to expose the top surface of the Si pillars, whose sidewalls remained covered with SiO_2. The process flow is described in more detail in reference [21]. The selective growth was then realized on the Si top surface of the pillars by choosing MBE growth conditions under which the Ge(Sn) adatoms nucleate exclusively on the Si top surface of the pillars while desorbing from the SiO_2 matrix according to previous studies in references [22], [23].

Two sets of samples were fabricated according to the parameters summarized in Tab. 1. The first set of samples consists of GeSn nano-islands with various island diameters that were deposited on p^--doped Si nano-pillars with a Boron (B) concentration of 10^{14} cm^{-3}. The second set of samples was grown on n^{++}-doped Si nano-pillars with a high Antimony (Sb) concentration of 10^{19} cm^{-3}. Both nano-patterned Si substrates exhibit the same dimensions (height and width of the nano-pillars as well as pitch size). After wet chemical and in-situ thermal cleaning of the substrate, the GeSn nano-islands were grown by co-evaporation of Ge and Sn with a Ge growth rate of 7.0 ± 1.5 nm/min at a substrate temperature of 600 °C. This particular choice of deposition temperature results in a GeSn accumulation that is almost exclusively restricted to the top of the Si pillars, i.e. selective growth of GeSn on Si. Further details of this process are described in detail elsewhere [22], [23]. We note that the average Sn content of all four GeSn samples was found to be low (≈2 at.%). As will be discussed, in our case the introduction of Sn into the nano-islands does not qualitatively influence device operation compared to pure Ge nano-islands. As a result, the remaining samples of the series were grown using pure Ge. The Ge nano-islands were

Accepted Manuscript

1 2 3 4 5 6 7 8 9 10 11 12 13 14 15 16 17 18 19 20 21 22 23 24 25 26 27 28 29 30 31 32 33 34 35 36 37 38 39 40 41 42 43 44 45 46 47 48 49 50 51 52 53 54 55 56 57 58 59 60

Accepted Manuscript

deposited at 850 °C with a deposition rate of about 1.0 nm/min according to reference [24]. The island diameter was varied by adjusting the deposition time, i.e. the total amount of Ge(Sn) deposited on the substrate.

Table 1: Overview of sample IDs of Ge and GeSn nano-islands grown on p^-- and n^{++}-doped Si nano-pillars with various island diameters. The sample name ID indicates the type of the nano-islands (Ge or GeSn) and the island diameter, e.g. sample GeSn120 consisting of GeSn nano-islands with a diameter of 120 nm.

Substrate doping	Device ID	Island diameter (nm)	Growth temperature (°C)	Al thickness (nm)
p^-	GeSn120	120	600	100
	GeSn155	155	600	80
	GeSn190	190	600	100
n^{++}	GeSn140	140	600	75
	Ge200	200	850	
	Ge160	160	850	
	Ge130	130	850	

The crucial aspect in photodetector fabrication is the deposition of contacts to the nano-scale Ge(Sn) islands. Here, Al was chosen as a contact metal because of its CMOS compatibility and contacts were structured using a lift-off process. In order to simultaneously contact the nano-islands and achieve plasmonic enhancement, we used Al evaporation in a physical vapor deposition (PVD) system in which the samples were inclined. During this deposition step, the nano-islands themselves act as a shadow mask, which results in the formation of nano-crescent holes in the Al film adjacent to each nano-island. The dimensions of the nano-crescent holes are influenced by the size of the Ge(Sn) nano-islands but can also be adjusted by varying the angle of inclination of the samples. For our samples, after an optical lithography step, Al was evaporated by an electron beam under an inclined angle of about 30°. A similar approach was used previously to fabricate nano-crescent holes by nanosphere lithography and in the fabrication of InGaAs nano-pillar photodetectors [25]. Finally, a backside contact consisting of Al was deposited. The Ge(Sn) photodetectors are shown schematically in Figure 1.

2.2 Characterization

Structural characterization of the nano-islands was performed based on scanning-electron microscopy (SEM) and transmission electron microscopy (TEM) measurements. To measure the photocurrent, the samples were glued onto copper plates using conducting silver paste and contacted from the top as well as from the backside. Device characterization was carried out by measuring responsivity spectra under illumination with a supercontinuum laser source. In the photocurrent measurement set up an optical light fiber was used to illuminate the sample in vertical incidence with light from a supercontinuum light source combined with an acousto-optical filter (see Figure 1). Responsivity spectra R_{opt} for wavelengths between 650 nm and 1100 nm were obtained in step sizes of 5 nm at room temperature in air according to

$$R_{opt} = \frac{I_{\lambda,on} - I_{\lambda,off}}{\Phi_\lambda} \quad . \qquad (1)$$

1 2 3 4 5 6 7 8 9 10 11 12 13 14 15 16 17 18 19 20 21 22 23 24 25 26 27 28 29 30 31 32 33 34 35 36 37 38 39 40 41 42 43 44 45 46 47 48 49 50 51 52 53 54 55 56 57 58 59 60

Here, $I_{\lambda,on}$ ($I_{\lambda,off}$) is the diode current with (without) illumination. For all measurements, a fixed external bias of 0 V was selected. The optical power output of the fiber Φ_{λ} was measured with a reference detector with a known optical responsivity. More details of the experimental set-up can be found in reference [18]. For the photocurrent measurements two illumination spots were selected for each device. Position A is assigned to the region where the sample surface is partially covered by the Al metallization layer, whereas position B corresponds to a region in which no Al cover layer is present (Figure 1 (a)). This was used for reference measurements.

2.3 Simulation

To provide a better understanding of the working principles of the fabricated devices two different simulation methods were used: (i) the software COMSOL was used to determine the band alignment of the doped heterostructure layers and (ii) the finite-element code FDmax was used to calculate the spatial distribution of the electromagnetic fields within the nano-heterostructure as well as to calculate absorption spectra.

(i) To understand the band alignment in the device and the influence of differently doped Si substrates on device operation, simulations were performed using the software COMSOL (Figure 5). An one dimensional geometry was assumed with a 100 nm thick Ge nano-island and 2 µm thick Si substrate. The bandgap of Ge (Si) was set to 0.66 eV (1.12 eV). Substrate doping concentrations of 10^{14} cm^{-3} (p^{-}-Si) and 10^{19} cm^{-3} (n^{++}-Si) were assumed. For Ge a carrier concentration was chosen with an average hole (electron) concentration of $5{\cdot}10^{16}$ cm^{-3} (10^{10}-10^{11} cm^{-3}): in intrinsic Ge, the presence of defects has been known to effectively introduce unintentional p-type doping with a defect concentration in that range. For the metal-semiconductor interface, the Schottky barrier height for the Si-Al interface was set to 0.69 eV [26] and for the Ge-Al interface to 0.70 eV [27]. It is known that Ge-metal contacts exhibit Fermi level pinning, i.e. the Fermi level E_f at Ge-metal interfaces remains close to the valence band edge irrespectively of the metal work function [28], [29], [30]. As a result of the incorporation of 2 at.% Sn the bandgap of GeSn is slightly decreased with respect to that of pure Ge, however, because of the low Sn content we can assume that its influence on the Schottky barrier height is negligible and that the behavior of the Ge and GeSn nano-islands in the respective devices is comparable.

(ii) The calculations of the electromagnetic field distributions in the nano-island photodetector were performed with the finite-element code FDmax, which has been developed for the analysis of photonic devices [31]. It provides a three-dimensional solution of the vectorial Helmholtz equation for the electromagnetic fields in frequency domain. Using a complex, dispersive permittivity for the materials, the absorbed power for any region of the simulation domain was determined. In our case, the relative absorbed power in single GeSn nano-islands (Figure 1 (c)) was studied with the permittivity taken from reference [31] and the Al thickness was set to 100 nm.

3. Results and discussion

Since the characterization of nano-island morphology and composition as a function of deposition parameters is discussed in detail in Ref. [22], [23], here, we focus on giving only the structural characterization results that are relevant to device operation. As will be discussed in detail in the

Accepted Manuscript

1 2 3 4 5 6 7 8 9 10 11 12 13 14 15 16 17 18 19 20 21 22 23 24 25 26 27 28 29 30 31 32 33 34 35 36 37 38 39 40 41 42 43 44 45 46 47 48 49 50 51 52 53 54 55 56 57 58 59 60

Accepted Manuscript

following section, the wavelength-dependent responsivity is strongly influenced by the metallization as well as the nano-island size. The structural characterization results of *GeSn140* can be found in Figure 2 (a-c) using scanning transmission electron microscopy (STEM) in bright field mode (BF) as well as energy dispersive x-ray spectroscopy (EDX) mapping the chemical composition. The pyramidal shaped GeSn nano-islands exhibit an average Sn content of 1.4 ± 0.5 at.%. In contrast, the Ge nano-islands have a spherical shape that is bound by many small facets, similarly to what was obtained in the previous study of Niu et al. [24]. No Sn contamination was detected in the Ge nano-islands (Figure 2 (d-f)). The scanning electron microscopy (SEM) and the TEM micrographs of the Ge(Sn) nano-islands deposited on p^-- and n^{++}-Si substrate after metallization reveal that the Ge(Sn) nano-islands are mostly covered with Al (Figure 3). Furthermore, the nano-crescent holes created adjacent to the Ge(Sn) nano-islands due to the shadowing effect of the nano-islands themselves are clearly visible. The thicknesses of the Al top layer for all samples are given in Table 1. Since all nano-islands grown on n^{++}-Si substrates were metallized simultaneously in one process, the same Al layer thickness is assumed for *Ge130*, *Ge200* and *GeSn140*.

3.1 Electrooptical measurements

Electrical characterization results show diode behavior for all GeSn nano-island devices (Figure 4). The weakly oscillating behavior of the current under reverse bias for devices on p^--substrates can be attributed to vibrations and subsequent contact problems during the measurement, which were exacerbated by the low thickness of the metal layer. The I/V curves of the GeSn nano-island devices on n^{++}-doped Si substrates show only a weak asymmetry when comparing the positive and negative bias regions. This is in agreement with COMSOL simulation results, which show the depletion region to extend throughout the Ge nano-island in case of the n^{++}-doped Si substrate (Figure 5 (b)). Hence, in this configuration of a p Ge/ n^{++}-Si heterojunction the current cannot be blocked efficiently under reverse bias conditions (see Figure 5 (d)). As a consequence, the current under reverse bias is almost three orders of magnitude larger than in the case of devices fabricated on p^--doped Si substrates. Under forward bias, devices on n^{++}-doped Si substrates also show currents that are more than two orders of magnitude larger than in the case of devices fabricated on p^--doped Si substrates (Figure 4). We attribute this to the large substrate resistance of the p^--doped Si substrates. Finally, simulation results show the position-dependent electric field at 0 V external bias for both p^-- and n^{++}-doped Si substrates to be non-zero within the Ge nano-islands as well as close to the Al backside contact (Figure 5 (c), (d)). Electron-hole generation by incident light can, thus, a priori be expected to contribute to a measurable photocurrent in both regions.

Electrooptical characterization results for all devices on p^-- and n^{++}-doped Si substrates are shown in Figure 6. When illuminated at position A (see Figure 1 (a)), all GeSn nano-island devices on p^--doped Si substrates feature an enhanced optical responsivity at an illumination wavelength of ≈ 680 nm (peak 1 in Figure 6 (a)) independently of the island size. Interestingly, the devices with the smallest nano-islands *GeSn120* have the highest R_{opt} of about 0.1 A/W, which is almost twice the responsivity obtained from *GeSn190* with highest island diameter. At an illumination wavelength of ≈1000 nm (peak 3) a second peak can be observed for all devices. Here, the peak responsivity again varies strongly with island size. Furthermore, device *GeSn155* exhibits an additional resonance peak at an illumination wavelength of ≈850 nm (peak 2). The optical responsivity at position A of all GeSn and Ge nano-island devices grown on

1 2 3 4 5 6 7 8 9 10 11 12 13 14 15 16 17 18 19 20 21 22 23 24 25 26 27 28 29 30 31 32 33 34 35 36 37 38 39 40 41 42 43 44 45 46 47 48 49 50 51 52 53 54 55 56 57 58 59 60

n^{++}-Si pillar substrates are illustrated in Figure 6 (b). The fluctuations in responsivity of some samples in the wavelength region between 750 nm and 880 nm can be attributed to a low signal-to-noise ratio. All Ge and GeSn nano-island devices show a pronounced increase in optical responsivity towards the lower limit of the investigated wavelength range (for illumination wavelengths of ≈650 nm, peak 1). This suggests a signal peak at <650 nm outside the range of the experimental setup, which is limited to wavelengths between 650 nm and 2000 nm. Similarly as in case of the nano-islands grown on p^--Si substrate, the devices with the smallest Ge nano-islands (sample *Ge130*) exhibit the largest optical responsivity (up to 0.09 A/W). For illumination wavelengths of ≈950 nm (peak 3) a slight increase of the optical responsivity can be observed for all devices. For our samples, responsivity peaks in the spectra occur at photon energies that are well above the bandgap energy of Ge or GeSn, making the qualitative influence of the material composition on the responsivity indeed negligible. Quantitatively, we could expect the introduction of Sn to increase responsivity at all wavelengths compared to pure Ge [32]. However, a quantitative comparison of our Ge nano-island devices with the GeSn nano-island devices is difficult because the nano-island geometries are different – the strong influence of island geometry on responsivity spectra will be discussed in more detail in the following subsection. Finally, we note that device responsivities show a dependence on the polarization of the incident light. In our measurements, the orientation of the optical fiber is adjusted so as to maximize responsivities in the wavelength range of ≈650 – 750 nm for all samples (see Supplementary Information).

Since electron-hole generation within the Si wafer can, in principle, contribute to a photocurrent, the influence of the substrate on the responsivity measurement results has to be assessed. To this end we compare the measured R_{opt} of sample *GeSn120* as well as sample *GeSn140* illuminated at position A and B (Figure 7). If the photocurrent originates exclusively from the Ge(Sn) nano-islands, a signal of the GeSn nano-islands is only expected under illumination at position A. In this case, the generated charge carriers can diffuse towards the metal contacting the Ge(Sn) nano-islands before recombination can occur. Indeed, the optical responsivity for sample *GeSn140* (n^{++}-doped Si substrate) under illumination at position B is zero at all wavelengths. For the case of the p^--Si substrate (sample *GeSn120*) illuminated at position B, however, the wavelength-dependent responsivity is non-zero and shows a peak at ≈ 1000 nm. Based on the peak shape we argue that this contribution to photocurrents originates specifically from charge carriers generated within the Si substrate close to the Al backside contact. In this wafer region, a non-zero electric field (Figure 5 (c)) induces the separation of charge carriers followed by diffusion to the contact. The drop in optical responsivity for wavelengths >1000 nm is a consequence of the bandgap of Si at 1100 nm (1.12 eV), which acts as a cut-off for absorption at higher wavelengths. The drop at lower wavelengths can be explained with an increase in absorption of bulk Si, which prevents the incident light from fully penetrating through the wafer. In comparison, the measured responsivities of sample *GeSn120* illuminated at position A only exhibit a weak shoulder at ≈1000 nm incident light wavelength. Indeed, in this case the incident light has to propagate though the comparatively small nano-crescent apertures, which leads to scattering and strongly reduces the light intensity within the Si wafer in the vicinity of the backside contact. Finally, in the case of the n^{++}-doped Si substrate, strong free carrier absorption prevents the incident light from fully penetrating into the Si wafer to the backside and contributions from the substrate to the photocurrent are effectively suppressed. For all samples, we attribute the responsivity peaks mainly to the influence of the Ge(Sn) nano-islands.

Accepted Manuscript

1 2 3 4 5 6 7 8 9 10 11 12 13 14 15 16 17 18 19 20 21 22 23 24 25 26 27 28 29 30 31 32 33 34 35 36 37 38 39 40 41 42 43 44 45 46 47 48 49 50 51 52 53 54 55 56 57 58 59 60

In view of the small size of the Ge(Sn) nano-islands, the maximum responsivity that can be measured in our devices is high. While a comparison with bulk Ge photodiodes is difficult because of the differences in device geometry and layer structure, we nonetheless note that e.g. in vertical bulk Ge PIN photodiodes grown by MBE and with a thickness of 300 nm of the intrinsic Ge layer, a responsivity of 0.2 – 0.3 A/W can be expected at illumination wavelengths of ≈650 nm [33]. Another notable feature of the responsivity spectra is the occurrence of peaks. It is interesting to note that while peak positions for the Ge(Sn) nano-islands on p^-- and n^{++}-doped Si substrates are at comparable wavelengths, the dependence of the peak responsivity on island diameter varies significantly. In our nanoscale structures, the wavelength dependence of our spectra can, in principle, originate from the geometry of the subwavelength-sized Ge(Sn) nano-islands, from local surface plasmon resonances (LSPRs) generated in the metal contact layer or from ordering effects of the square lattice arrangement of the nano-islands. Absorption in the sub-wavelength nano-islands themselves can be dominated by the resonant excitation of discrete photonic modes within the islands, the so-called leaky mode resonances (LMRs) [34]. Furthermore, in our devices, both the crescent-shaped nano-holes in the Al metallization adjacent to the Ge(Sn) nano-islands and the Al cap covering the nano-islands can support LSPRs that could enhance light absorption at specific wavelengths. While those effects play a role for individual Ge(Sn) nano-islands, the introduction of periodicity by growing the Ge(Sn) nano-islands on square lattices of Si nano-pillars can, in principle, introduce additional effects such as photonic crystal Bloch modes [35] or surface plasmon polariton modes supported by the array of nano-crescent Al holes [36]. For our samples, as Figure 3 shows, the positioning of the Ge(Sn) nano-islands on the Si nano-pillars as well as their size is subject to variations. As a result, the Ge(Sn) nano-islands do not, in fact, form a regular lattice and we exclude the influence of lattice ordering in the following discussion.

3.2 Simulation of absorption spectra

To analyze the measured responsivity spectra further, the absorptivity of the GeSn nano-islands was evaluated theoretically. Here, we focus our comparison of simulation and experimental data on samples grown on p^--doped Si substrates. For these samples, the peak structure is fully apparent in the measured spectra, which facilitates comparison between experimental and simulation results. The simulations qualitatively reproduce both the number of peaks and the experimentally observed weak dependence of the peak position on island size (Figure 8). Quantitative differences in the exact peak positions and magnitudes can be attributed to experimental imperfections such as non-spherical nano-island geometries, variations in island size and shape, roughness in the metal layer and local changes in metal thickness. The simulation results confirm that increasing the diameter of the GeSn nano-islands from 120 nm to 190 nm only results in a slight shift of the peak positions. This weak dependence of peak positions on island diameter makes it unlikely that the peak structure originates from the LMRs of the subwavelength Ge(Sn) nano-islands, whose wavelength dependence is strongly influenced by island size [34]. We also note that the absorption in the Si substrate is not included in the calculated absorptivity, further indicating that while we cannot fully rule out any influence of the Si substrate on measured responsivities for nano-islands on p^--substrates, the responsivity spectra at wavelengths above 900 nm clearly show contributions from the nano-islands.

Accepted Manuscript

1
2
3
4
5
6
7
8
9
10
11
12
13
14
15
16
17
18
19
20
21
22
23
24
25
26
27
28
29
30
31
32
33
34
35
36
37
38
39
40
41
42
43
44
45
46
47
48
49
50
51
52
53
54
55
56
57
58
59
60

In order to assess the influence of the LSPRs on the responsivity spectra, we investigated the distribution of the intensity of the electric field within devices with nano-island diameters of 120 nm for x-polarized, vertically incident light at a resonance wavelength of 680 nm (corresponding to peak 1) as well as at 900 nm. Intensity plots along cuts through the center of the investigated system perpendicular to the y-axis show hot spots within and around the nano-crescent apertures as well as at the interface between the metal covering the top of the island and the island itself (Figure 9). The regions of enhanced electromagnetic field intensities within the nano-islands (highlighted in parts (a) and (d) of Figure 9) are absent in a cross-sectional intensity plot for a nano-island without the Al metallization (Figure 9 (c)). LSPRs excited by the incoming light within the nano-crescent aperture as well as in the section of the Al metallization covering the island, which acts as a metallic nanoantenna [36], induce local field enhancement within the nano-islands. This leads to an increase in absorption within the Ge(Sn) nano-islands partly covered with Al. In our case, a strong resonance occurs at 680 nm, where the absorptivity is governed by the transmission behavior of the nano-crescent aperture. For long slits, it has been shown [37] that resonances occur for the perpendicular (x-) polarization case, which show a non-trivial dependence on metal thickness, periodicity, and slit width. At 920 nm and 1080 nm, two more resonances occur, where the field intensity in the nano-island is enhanced compared to the case without metal. The calculation of the field distribution in Figure 9 (d) shows that at > 800 nm the plasmons are excited in the Al cap layer at the Al-Ge interface.

Finally, the wavelength-dependence of the photocurrent generated within the Ge(Sn) nano-island devices is influenced not only by the LSPRs alone but rather by the interplay of local electric field enhancement by LSPRs and the electric field distribution resulting from doping (Figure 5). While the nano-islands both on p^--and on n^{++}-doped substrates exhibit enhanced responsivities at incident wavelengths of 700 nm and below, the size-dependent behavior of the nano-islands is markedly different at larger wavelengths. At these wavelengths, experimentally measured peak responsivities of nano-islands on n^{++}-substrates show a much weaker dependence on island size (Figure 6 (b)) than predicted by simulation (Figure 8 (b)). We attribute this behavior to the fact that as doping strongly influences the position-dependent electric fields within the nano-islands (Figure 5), the efficiency with which photogenerated carriers in different regions of the nano-islands contribute to photocurrents can vary.

If LSPRs in the contact metal have a strong influence on the wavelength dependent responsivity spectra, changes in the geometry of the metal layer, most notably its thickness, should modify the responsivity spectra. Indeed, we find that both by varying island diameter and by varying the Al thickness on top of the GeSn nano-islands the absorption spectra can be strongly modified (Figure 10). While the GeSn nano-island shows no enhanced absorption without a plasmonic Al antenna, the dependence of the absorption spectra on island diameter as well as Al thickness is non-trivial. Figure 10 (a) shows the absorption spectra for GeSn with island diameters of 120 nm. Varying the thickness of the Al top cover drastically changes the absorption peaks in the investigated wavelength regime and the device can be tuned from broadband detection (for an Al thickness of 120 nm) to a regime in which high absorption only occurs in a limited wavelength range (for an Al thickness of 100 nm). Changing the nano-island diameter to 160 nm leads to overall lower absorption within the nano-island (Figure 10 (b)). In this case, at Al thicknesses between 60 nm and 100 nm, a double peak at about 975 nm (peak 2) and 1105 nm (peak 3) can be observed with different peak intensities depending on the Al thickness. One single peak

Accepted Manuscript

1 2 3 4 5 6 7 8 9 10 11 12 13 14 15 16 17 18 19 20 21 22 23 24 25 26 27 28 29 30 31 32 33 34 35 36 37 38 39 40 41 42 43 44 45 46 47 48 49 50 51 52 53 54 55 56 57 58 59 60

at about 1105 nm (peak 3) can be observed when the Al top layer is 120 nm thick. This establishes the Al thickness as an additional parameter for tuning wavelength-dependent responsivities.

4. Conclusion

In conclusion, we have demonstrated that subwavelength-sized Ge(Sn) nano-islands can be utilized as active material for a photodetector in the visible/NIR regime. Our devices were realized using CMOS-compatible materials, paving the way for a future integration in Si technology. Using local field enhancement by LSPRs, we were able to achieve a responsivity of up to 0.1 A/W under vertical illumination at ≈700 nm. For our devices, the evaporation of Al at an off-angle on top of the Ge(Sn) nano-island array was a successful strategy to contact the nano-islands while simultaneously forming self-aligned antennas with nano-crescent holes adjacent to the nano-islands.

In principle, the subwavelength dimensions of the nano-islands enable the excitation of optical modes at discrete frequencies (leaky modes). Furthermore, plasmonic excitations in nanostructures within the Al contact contribute to the wavelength-dependence of the responsivity. As a result of comparing measurements with three-dimensional simulations of the electric field distribution we found that in our devices, specifically the excitation of LSPRs in the nano-crescent holes as well as in the Al shell layer partially covering the nano-islands is at the origin of the comparatively high responsivities in arrays of subwavelength-sized Ge(Sn) nano-islands.

We find that the wavelength-dependent responsivity spectrum is sensitive to substrate doping and photodetector geometry, especially parameters of the Al metallization such as its thickness, which influence the LSPRs that can be generated in our devices. This opens up promising avenues towards further increasing device responsivity and modifying its wavelength-dependence towards obtaining efficient nanoscale Ge(Sn)-photodetectors directly integrated on Si. Depending on the possible application, either a high responsivity in a limited wavelength range (e.g. for optical data transmission) or broadband photodetection (e.g. for solar cells) could be required. Interestingly, our simulation results indicate that it could be possible to fine-tune our devices for either scenario by adjusting geometry parameters (island diameter and metal thickness). We could also exploit surface plasmon polariton modes in order to influence device responsivity, provided that the lattice periodicity of our Ge(Sn) nano-islands can be improved. Finally, further increasing the Sn content in our nano-islands by adjusting growth conditions could be a strategy to increase responsivity and, as a consequence, improve device performance. Our results, thus, can be a starting point for utilizing Ge(Sn) nano-islands as active optical material for photodetector integrated in Si technology for applications in which size reduction is of key importance.

Accepted Manuscript

Accepted Manuscript

References

[1] J. Wang and S. Lee, *Sensors,* vol. 11, p. 696, 2011.

[2] J. Michel, J. Liu and L. C. Kimerling, *Nature Photonics,* vol. 4, p. 527, 2010.

[3] D. Zubia and S. D. Hersee, *Journal of Applied Physics,* vol. 85, p. 6492, 1999.

[4] F. Montalenti, M. Salvalaglio, A. Marzegalli, P. Zaumseil, G. Capellini, T. U. Schülli, M. A. Schubert, Y. Yamamoto, B. Tillack and T. Schroeder, *Physical Review B,* vol. 89, p. 014101, 2014.

[5] K. Nozaki, S. Matsuo, T. Fuji, K. Takeda, M. ono, A. Shakoor, E. Kuramochi and M. Notomi, *Optica,* vol. 3, p. 483, 2016.

[6] L. Novotny and N. Van Hulst, *Nature Photonics,* vol. 5, p. 83, 2011.

[7] V. Giannini, A. I. Fernández-Domínguez, S. C. Heck and S. A. Maier, *Chemical Review,* vol. 111, p. 3888, 2011.

[8] N. C. Lindquist, P. Nagpal, K. M. McPeak, D. J. Norris and S.-H. Oh, *Reports on Progress in Physics,* vol. 75, p. 036501, 2012.

[9] J. N. Anker, W. P. Hall, O. Lyandres, N. C. Shah, J. Zhao and R. P. Van Duyne, *Nature Materials,* vol. 7, p. 442, 2008.

[10] H. R. Stuart and D. G. Hall, *Applied Physics Letters,* vol. 69, p. 2327, 1996.

[11] S. Pillai, K. R. Catchpole, T. Trupke and M. A. Green, *Journal of Applied Physics,* vol. 101, p. 093105, 2007.

[12] S. Pillai, K. R. Catchpole, T. Trupke, G. Zhang and M. A. Green, *Applied Physics Letteres,* vol. 88, p. 161102, 2006.

[13] A. Dorodnyy, Y. Salamin, P. Ma, P. Vukajlovic, N. Lassaline, D. Mikulik, P. Romero-Gomez, A. Fontcuberta i Morral and J. Leuthold, *IEEE Journal of Selected Topics in Quantum Electronics,* vol. 24, p. 1, 2018.

[14] S. C. Lee, S. Krishna and S. R. J. Brueck, *Optics Express,* vol. 17, p. 23160, 2009.

[15] T. Ishi, *Japanes Journal of Applied Physics,* vol. 44, p. L3364, 2005.

[16] J. A. Shackleford, R. Grote, M. Currie, J. E. Spanier and B. Nabet, *Applied Physics Letters,* vol. 94, p. 083501, 2009.

[17] L. Augel, Y. Kawaguchi, S. Bechler, S. Körner, J. Schulze, H. Uchida and I. A. Fischer, *ACS Photonics,* no. 5, p. 4586, 2018.

[18] I. A. Fischer, L. Augel, T. Kropp, S. Jitpakdeebodin, N. Franz, F. Oliveira, E. Rolseth, T. Maß, T. Taubner and J. Schulze, *Applied Physics Letters,* no. 108, p. 071108, 2016.

[19] L. Tang, S. E. Kocabas, S. Latif, A. K. Okyay, D.-S. Ly-Gagnon, K. C. Saraswat and D. A. B. Miller, *Nature Photonics,* vol. 2, p. 226, 2008.

[20] L. Tang, D. A. Miller, A. K. Okyay, J. Matteo, Y. Yuen, K. C. Saraswat and L. Hesselink, *Optics Letters,* vol. 31, p. 1519, 2006.

[21] O. Skibitzki, I. Prieto, R. Kozak, G. Capellini, P. Zaumseil, Y. A. R. Dasilva, M. D. Rossell, R. Erni, H. von Känel and T. Schroeder, *Nanotechnology,* vol. 28, p. 135301, 2017.

[22] V. Schlykow, W. M. Klesse, G. Niu, N. Taoka, Y. Yamamoto, O. Skibitzki, M. R. Barget, P. Zaumseil, H. von Känel, M. A. Schubert, G. Capellini and T. Schroeder, *Applied Physics Letters,* vol. 109, p. 202102, 2016.

[23] V. Schlykow, P. Zaumseil, M. A. Schubert, O. Skibitzki, Y. Yamamoto, W. M. Klesse, Y. Hou, M. Virgilio, M. De Seta, L. Di Gaspare, T. Schroeder and G. Capellini , *Nanotechnology,* vol. 29, p. 415702, 2019.

[24] G. Niu, G. Capellini, M. A. Schubert, T. Nierman, P. Zaumseil, J. Kratzer, H. M. Krause, O. Skibitzki, M. Lehmann, Y. H. Xie, H. Von Känel and T. Schroeder, *Scientific Report,* vol. 6, p. 22709, 2016.

[25] P. Senanayake, C.-H. Hung, J. Shapiro, A. Scofield, A. Lin, B. S. Williams and D. L. Huffaker, *Optics Express,* vol. 20, p. 25489, 2012.

[26] A. Yu and C. Mead, *Solid-State Electronics,* vol. 13, p. 97, 1970.

[27] R. Lieten, V. Afanas'ev, N. Thoan, S. Degroote, W. Walukiewicz and G. Borghs, *Jounral of the Electrochemical Society,* vol. 158, p. H358, 2011.

[28] D. R. Gajula, P. Baine, M. Modreanu, P. Hurley, B. Armstrong and D. McNeill, *Applied Physics Letters,* vol. 104, p. 012102, 2014.

[29] T. Nishimura, K. Kita and A. Toriumi, *Applied Physics Letters,* vol. 91, p. 123123, 2007.

[30] A. Dimoulas, P. Tsipas, A. Sotiropoulos and E. K. Evangelou, *Applied Physics Letters,* vol. 89, p. 252110, 2006.

[31] F. Römer, O. Chinellato, P. Arbenz and B. Witzigmann, *Journal of Optical and Quantum Electronics,* vol. 39, p. 341, 2007.

Accepted Manuscript

1
2
3
4
5
6
7
8
9
10
11
12
13
14
15
16
17
18
19
20
21
22
23
24
25
26
27
28
29
30
31
32
33
34
35
36
37
38
39
40
41
42
43
44
45
46
47
48
49
50
51
52
53
54
55
56
57
58
59
60

[32] R. Roucka, R. Beeler, J. Mathews, M.-Y. Ryu, Y. K. Yeo, J. Menéndez and J. Kouvetakis, *Journal of Applied Physics,* vol. 109, p. 103115, 2011.

[33] M. Kaschel, M. Oehme, O. Kirfel and E. Kasper, *Solid-State Electronics,* vol. 53, p. 909, 2009.

[34] Y. Yu and L. Cao, *Optics Express,* vol. 20, p. 13847, 2012.

[35] K. T. Fountaine, W. S. Whitney and H. A. Atwater, *Journal of Applied Physics,* vol. 116, p. 153106, 2014.

[36] P. Senanayake, C.-H. Hung, J. Shapiro, A. Lin, B. Liang, B. S. Williams and D. L. Huffaker, *Nano Letters,* vol. 11, p. 5279, 2011.

[37] Y. Pang, C. Genet and T. W. Ebbesen, *Optics Communication,* vol. 280, p. 10, 2007.

[38] J. Xie, J. Tolle, V. R. D. D'Costa, C. Weng, A. V. G. Chizmeshya, J. Menendez and J. Kouvetakis, *Solid State Electronics,* vol. 53, p. 816, 2009.

Accepted Manuscript

1
2
3
4
5
6
7
8
9
10
11
12
13
14
15
16
17
18
19
20
21
22
23
24
25
26
27
28
29
30
31
32
33
34
35
36
37
38
39
40
41
42
43
44
45
46
47
48
49
50
51
52
53
54
55
56
57
58
59
60

Figures

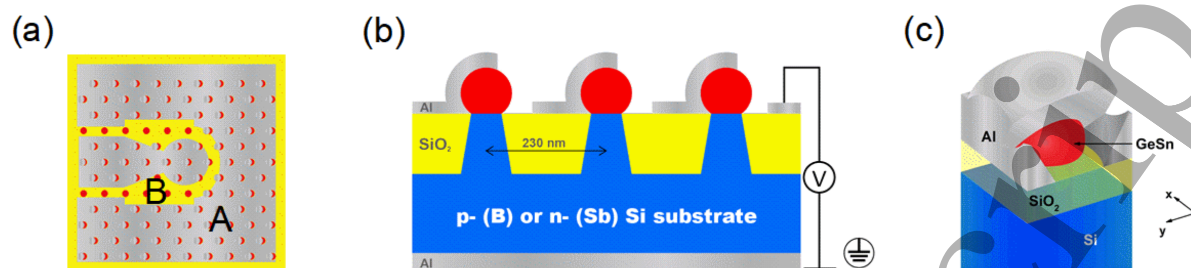

Figure 1: Schematic sketch of (a) top view of nano-island array with (A, position A) and without (B, position B) Al top contact. (b) cross section of nano-island/Si pillar photodetector with pitch size L = 230 nm. The nano-islands are partly covered with an Al layer featuring metal nano-crescent holes adjacent to the nano-islands. (c) 3-dimensional model of the absorption simulation. One GeSn island with varying diameter (120, 150, 190 nm) is illuminated by a linearly polarized plane wave from the top. The nano-island is partly covered by a 100 nm thick Al shell layer.

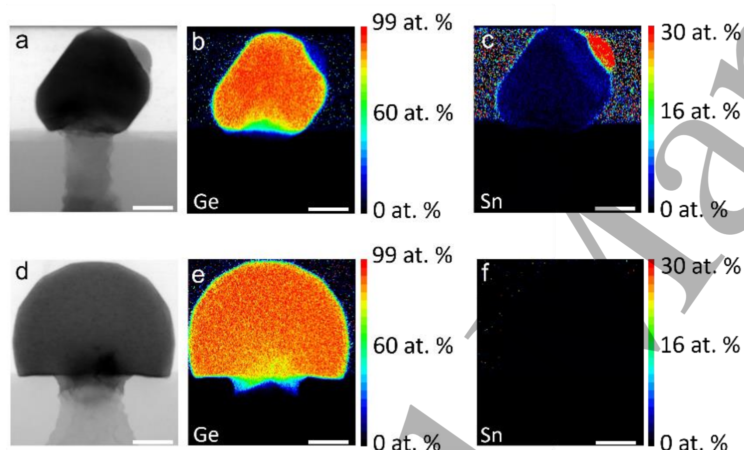

Figure 2: (a) STEM BF image, EDX map of (b) Ge and (c) Sn distribution of GeSn140. The average Sn content within the nano-island is 1.4±0.5 at.%. (d) STEM BF image, EDX map of (e) Ge and (f) Sn distribution of Ge160. No Sn contamination can be detected in the Ge nano-island. The scale bar of all images is 40 nm.

Accepted Manuscript

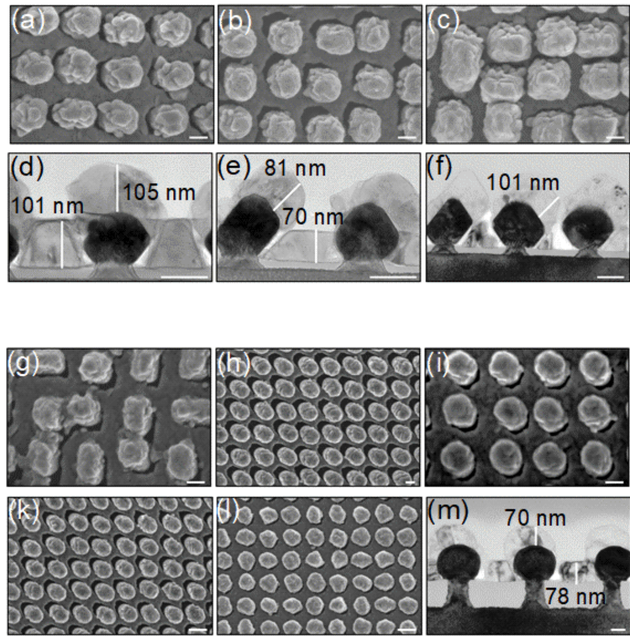

Figure 3: (a-f) Micrographs of nano-islands on p$^-$-Si substrate (a-f). SEM top view of (a) GeSn120, (b) GeSn155 and (c) GeSn190 after the evaporation of Al. TEM cross section images of (d) GeSn120, (e) GeSn155 and (f) GeSn190 with the corresponding height of the Al layer. The scale bar of all images corresponds to 100 nm. (g)-(m) Micrographs of nano-islands on n^{++}-Si substrate (g-l). SEM top view of (g) GeSn140, (h) Ge200 and (i) Ge130 with scale bar of 100 nm and (k,l) Ge160 with a scale bar of 200 nm at different positions on the sample. (m) TEM cross section images of Ge160 with the corresponding height of the Al layer with a scale bar of 50 nm.

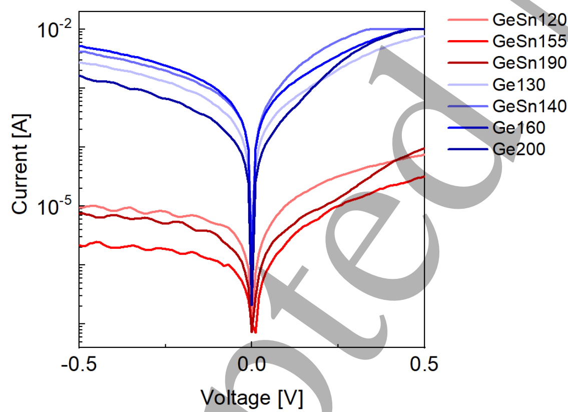

Figure 4: Measured I/V curves of all samples grown on p$^-$- (red colors) and n^{++}-Si substrate (blue colors). The current is measured applying a bias from -0.5 V to +0.5 V.

Accepted Manuscript

1
2
3
4
5
6
7
8
9
10
11
12
13
14
15
16
17
18
19
20
21
22
23
24
25
26
27
28
29
30
31
32
33
34
35
36
37
38
39
40
41
42
43
44
45
46
47
48
49
50
51
52
53
54
55
56
57
58
59
60

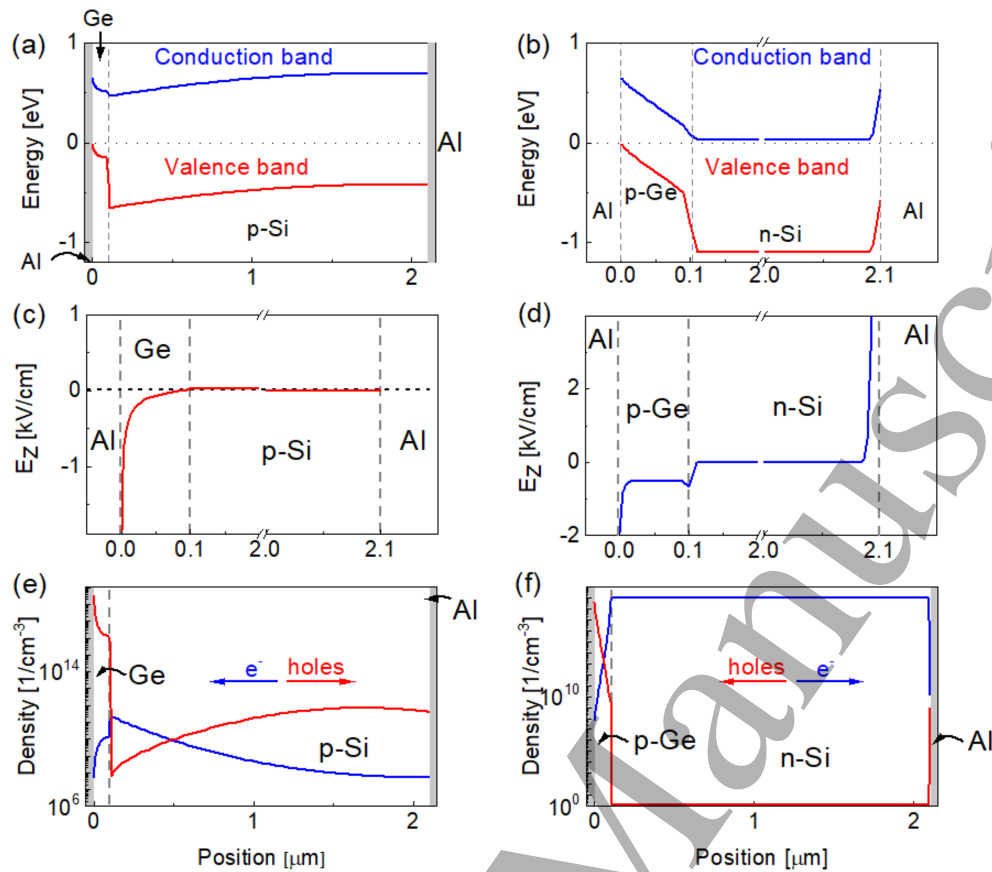

Figure 5: COMSOL simulation results at 0 V assuming a one-dimensional layer stack with 100 nm Ge and 2 µm Si substrate for the band alignment of Ge nano-islands on (a) p^--doped and (b) n^{++}-doped Si, the calculated spatial distribution of the electric field in the Al-Ge-Si-Al heterostructure using (c) p^-- or (d) n^{++}-doped Si substrate and the distribution of the carrier concentration in the nano-islands deposited on (e) p^-- and (f) n^{++}-doped Si pillars.

Accepted Manuscript

Accepted Manuscript

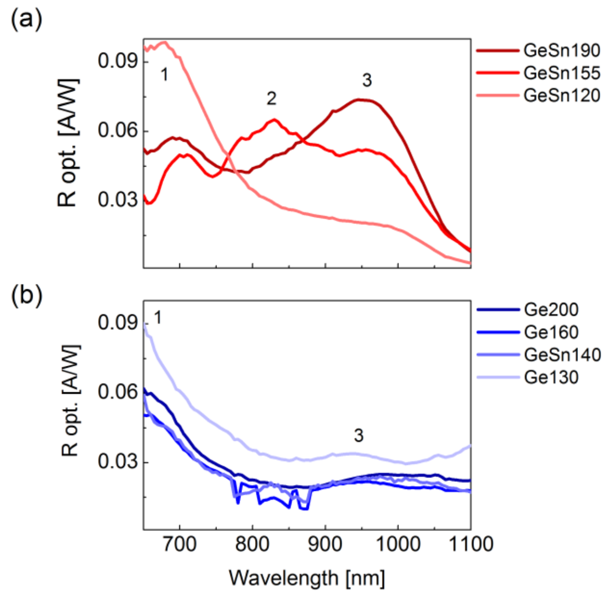

Figure 6: Responsivity spectra $R_{opt.}$ of Ge and GeSn nano-islands on (a) p^--Si substrate (red graphs) and (b) n^{++}-Si substrate (blue graphs) at position A depending on the wavelength. The increasing island size is indicated as darkening of the color. The different peaks are labeled with numbers from 1 to 3.

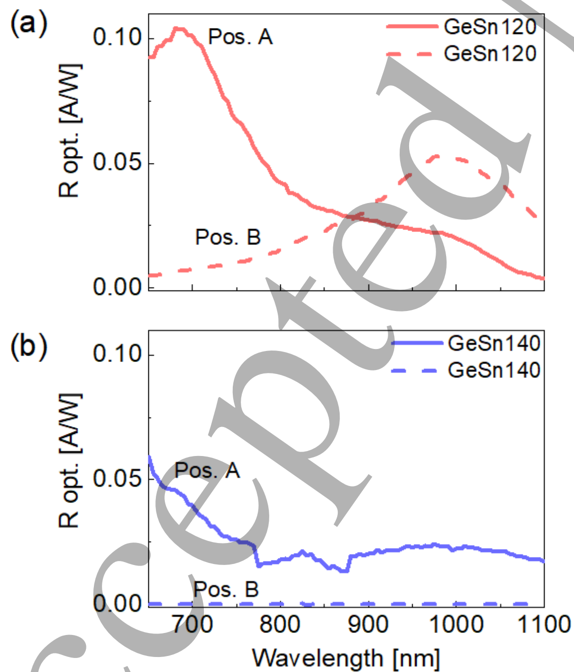

Figure 7: Wavelength-dependent responsivity spectra $R_{opt.}$ of (a) GeSn120 on a p^--Si substrate (red) and (b) GeSn140 on a n^{++}-Si substrate (blue). Position A (solid graph) corresponds to a region with Al, while at position B (dashed graph) no Al top layer is present.

1
2
3
4
5
6
7
8
9
10
11
12
13
14
15
16
17
18
19
20
21
22
23
24
25
26
27
28
29
30
31
32
33
34
35
36
37
38
39
40
41
42
43
44
45
46
47
48
49
50
51
52
53
54
55
56
57
58
59
60

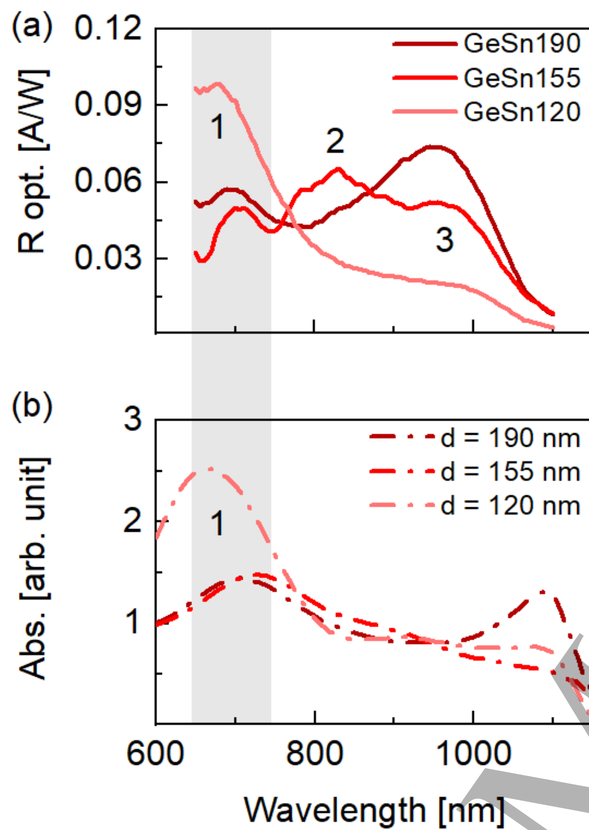

Figure 8: (a) Measured responsivity spectra of nano-islands grown on p⁻-Si substrate. (b) Calculated absorption spectra of GeSn nano-islands with varying diameters. The Al layer thickness is set to 100 nm in simulation. Characteristic peaks are labeled with numbers from 1 to 3.

Accepted Manuscript

1
2
3
4
5
6
7
8
9
10
11
12
13
14
15
16
17
18
19
20
21
22
23
24
25
26
27
28
29
30
31
32
33
34
35
36
37
38
39
40
41
42
43
44
45
46
47
48
49
50
51
52
53
54
55
56
57
58
59
60

Accepted Manuscript

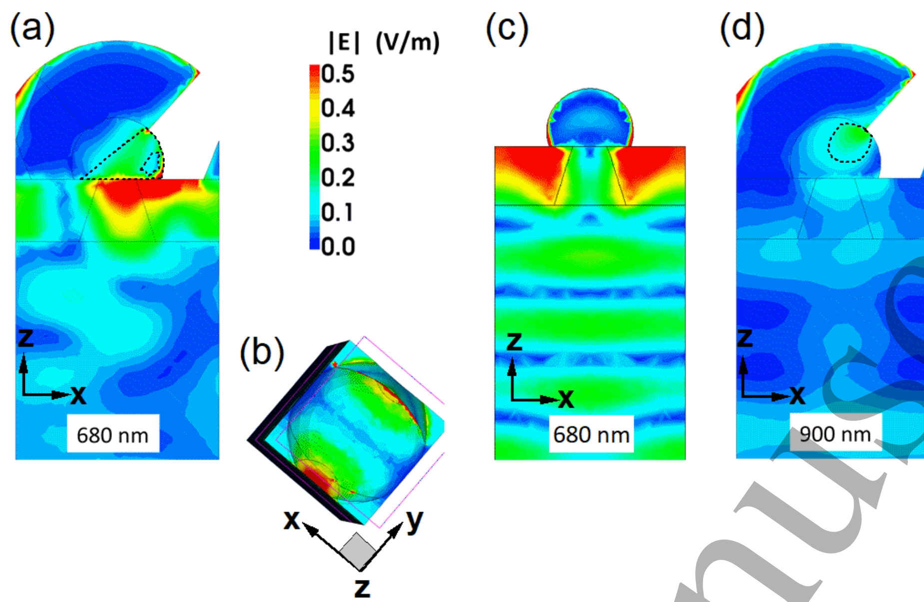

Figure 9: Calculated intensity of the electric field in case of a GeSn nano-island with a diameter of 120 nm and an illumination wavelength of (a)-(c) 680 nm and (d) 900 nm. Cross-sectional plots are shown in (a, c, d), while (b) shows a top view of the heterostructure. (a,b) and (d) show the distribution of the electric field in the presence of a 100 nm thick Al metallization. The regions of enhanced electric field intensities within the nano-island are highlighted with dashed lines in (a) and (d) and absent in the simulation result (c) for a GeSn nano-island without Al.

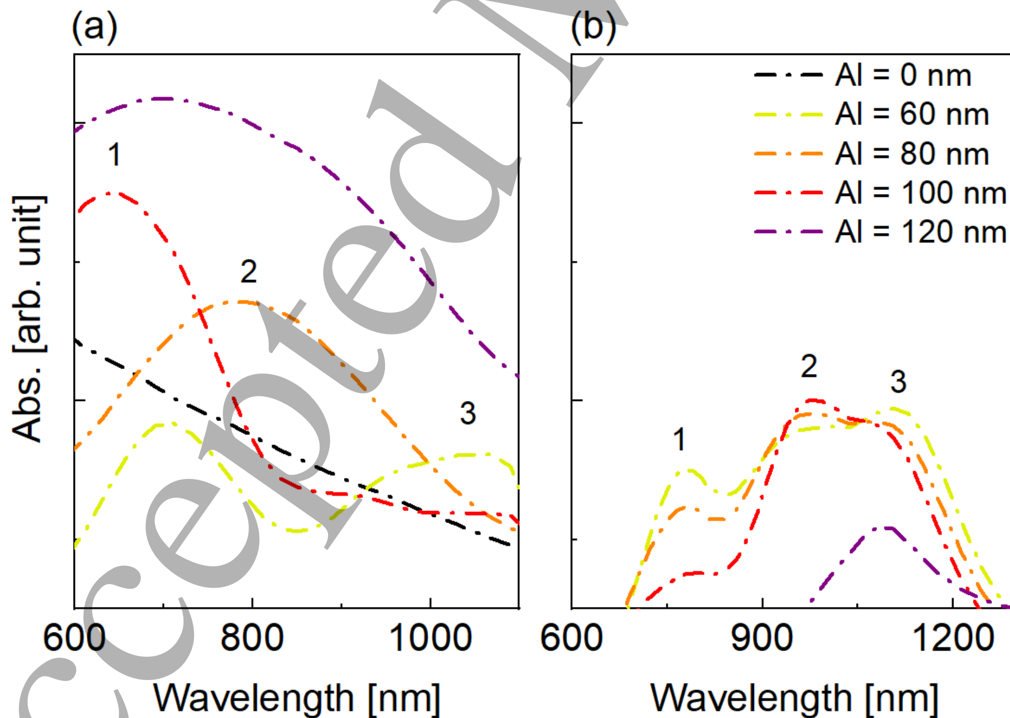

Figure 10: Calculated absorption spectra of a GeSn nano-island with a diameter of (a) 120 nm and (b) 160 nm for different Al thicknesses from 60 nm (yellow) to 120 nm (purple). The absorption spectrum of a nano-island without a Al top cover is indicated as a black line for comparison in (a). Characteristic peaks a labeled with numbers from 1 to 3.